Geophysical Research Letters

RESEARCH LETTER
10.1029/2019GL081932

Atmospheric Circulation Patterns Associated With Wildfires in the Monsoon Regions of China

Fengjun Zhao[1,2] and Yongqiang Liu[2]

[1]Research Institute of Forest Ecology, Environment and Protection, Chinese Academy of Forestry, Beijing, China, [2]Center for Forest Disturbance Science, USDA Forest Service, Athens, GA, USA

Key Points:
- We identified three atmospheric circulation patterns for wildfires in the monsoon regions of China
- These patterns contributed to wildfires by generating warmer and drier conditions or affecting moisture transport
- We showed that a circulation index based on these patterns had better prediction skills for monthly fire occurrence than local weather

Supporting Information:
- Supporting Information S1

Correspondence to:
Y. Liu,
yliu@fs.fed.us

Citation:
Zhao, F., & Liu, Y. (2019). Atmospheric circulation patterns associated with wildfires in the monsoon regions of China. *Geophysical Research Letters*, *46*, 4873–4882. https://doi.org/10.1029/2019GL081932

Received 7 JAN 2019
Accepted 4 APR 2019
Accepted article online 11 APR 2019
Published online 3 MAY 2019

Abstract Major atmospheric circulation patterns for wildfires have been identified in regions with boreal, Mediterranean, and semiarid climates. This study investigates such patterns in the monsoon regions of China, where the climate is controlled by multiple atmospheric systems and wildfires have large spatial variability. We identified three patterns. The first pattern was characterized by a high-pressure ridge in northeast China and contributed to wildfires by creating warmer and drier conditions. The second, meridional pattern contributed to wildfires in north, central, and south China by increasing dry air transport. The third, zonal pattern had a weaker westerly ridge and trough and contributed to wildfires in southwest China by decreasing the transport from westerly systems. We showed that a circulation index defined as the pressure difference between the positive and negative centers of fire-pressure correlations had higher monthly fire prediction skills for large fire occurrences than local weather.

Plain Language Summary Atmospheric circulation as a driver of wildfire changes spatially. This study investigated the circulation patterns associated with wildfires and their regional dependence in the monsoon regions of China. We identified three patterns. The first pattern of positive pressure anomalies contributed to wildfires in northeast China with a cool temperate monsoon climate. The second pattern of strong southerly airflows contributed to wildfires in north, central, and south China with a subtropical East Asian monsoon climate. The third pattern of strong westerly airflows contributed to wildfires in southwest China with a subtropical South Asian monsoon climate. We showed that a circulation index formed based on the circulation patterns had higher prediction skills for large fire occurrences than local weather.

1. Introduction

Atmospheric circulation is a fundamental control of wildfires by delivering and distributing energy, moisture, and momentum (Hostetler et al., 2018; Trouet et al., 2018; Wahl et al., 2019). Wildfires have increased in recent decades in many regions of the world due to climate change and human factors (Abatzoglou & Williams, 2016; Doerr & Santín, 2016; Flannigan et al., 2009; Gill & Stephens, 2009; Schoennagel et al., 2017; Westerling et al., 2006), leading to severe ecological, environmental, social, and economic consequences (Liu et al., 2014; Moritz et al., 2014; Nagy et al., 2018; Steelman, 2016). As a result, the demands for improving the capacity and accuracy of fire predictions have received increasing attention globally (Lagerquist et al., 2017; Turco et al., 2018). Identifying the atmospheric circulation patterns associated with wildfires is of great value for meeting the demands.

Major atmospheric circulation patterns associated with wildfires have been identified in many regions of the world. These patterns are often related to prominent high pressure and ridge systems (Pereira et al., 2005; Peterson et al., 2010). For example, the high/low burned area years coincide with the positive/negative 500-hPa geopotential height ($Z500$) anomalies in subarctic Canada and Alaska (Fauria & Johnson, 2006; Hayasaka et al., 2016; Lagerquist et al., 2017; Skinner et al., 1999). The enhanced regional ridge and low atmospheric moisture are associated with high fire risks along the western coast of the United States (Nauslar et al., 2018; Trouet et al., 2009; Wise, 2016) and in southern Europe (Amraoui et al., 2013, 2015; Founda & Giannakopoulos, 2009; Papadopoulos et al., 2014; Paschalidou & Kassomenos, 2016; Ruffault et al., 2017), the two regions with a Mediterranean climate. Blocking highs are related to the major fires in semiarid southwestern Australia (O'Donnell et al., 2011). In a country or continent that is large enough to have a variety of climate types, atmospheric circulation patterns could vary spatially. For example, in addition to a high-pressure system as a dominant pattern in the first two empirical orthogonal function modes for

three continental regions in the United States, a low-pressure system and a pair of high and low systems in these modes dominate the other three regions (Heilman, 1995).

Monsoon is one of the major climate types in the world and prevails in East and South Asia, northern Australia, western and southeastern Africa, and southwestern North America. Monsoon climate is characterized by extremely hot and moist summers and cold and dry winters and is often connected to multiple planetary-scale atmospheric circulation systems. For example, the East Asian monsoon is associated with the northwestern Pacific High in the low latitudes and the westerly systems in the high latitudes (Ding & Chan, 2005). Thus, large spatial variability of wildfires and varied atmospheric circulation patterns for wildfires are expected in East Asia. Furthermore, monsoon climate has large interannual variability (Ha et al., 2012) due to the impacts of El Niño–Southern Oscillation, Pacific Decadal Oscillation, and other long-term atmospheric fluctuations (Yao et al., 2017), posing a great challenge to seasonal fire predictions.

Eastern China is part of the East and South Asian monsoon systems. Wildfires in this region vary dramatically in both space and time. Wildfires occur much more frequently in the south than in the north, while burned area has an opposite spatial pattern (Chang et al., 2015; Chen et al., 2017; Li et al., 2015; Lv et al., 2006; Tian et al., 2013). Many regions have two fire seasons in spring and fall and large interannual variability (Niu & Zhai, 2012; Yi et al., 2017) due to local, regional, and global atmospheric processes (Yao et al., 2017; Zhang et al., 2016). Efforts have been made to use atmospheric factors to predict seasonal fire activity in China (Chang et al., 2013; Li et al., 2014; Sun & Zhang, 2018). However, less attention has been paid to the circulation patterns associated with wildfires in the monsoon regions of China.

This study investigates the atmospheric circulation patterns associated with wildfires in the monsoon regions of China. The objectives are to identify the circulation patterns, understand their impacts on local weather, and develop wildfire predictors based on the circulation patterns and evaluate their skills against local weather.

2. Data and Methods

2.1. Study Area

The study area is the eastern part of China that is dominated by monsoon climate, where fire count and burned area account for 98%–99% of the national totals (Tables S1 and S2 in the supporting information). The study area is divided into the northeast (NE), north (NC), central (CC), south (SC), and southwest (SW) regions (Figure 1). NE has a cool temperate East Asian monsoon climate. NC, CC, and SC are under the control of the subtropical East Asian monsoon, while SW is under the control of the South Asian monsoon with alternate wet and dry seasons (Huang et al., 2017). (Note that Tibet and northwest China in Figure 1 are not controlled by monsoon climate and had minimal fire activity. Thus, they were not included in the study area.) NE and NC are often referred to as northern China and CC, SC, and SW as southern China. See supporting information for topography, vegetation, and weather features.

2.2. Data

A historical fire data set of the monthly fires in each of the mainland provinces of China with the most complete records from 1999 to 2017 was recently developed by the China National Forestry and Grassland Administration (http://english.forestry.gov.cn). The fire data were obtained from the China National Forest Fire Statistical System (http://60.205.191.66/FireReport/Account/LogOn?returnUrl=%2FFireReport%2F). Two fire properties, fire count (F_c) and burned area (F_a), were used in this study, and the values were converted from provincial to regional values.

The daily surface meteorological data in the study area, including maximum temperature, T_{max}, and relative humidity, RH, were obtained from more than 800 weather stations across China available in the China Meteorological Science Data Sharing Service Network (http://data.cma.cn/). Considering that wildfires occur only in vegetated lands, only the weather stations located in the areas covered by forest, grass, or shrubs (https://globalmaps.github.io/) were selected. The daily data were converted to monthly values, and regional values were obtained by averaging among the stations within each of the five regions. Other weather elements (average temperature, precipitation, wind speed, and vapor pressure deficit) were also analyzed. The results were not presented because they showed similar but often less close relationships with $Z500$ in compassion with T_{max} and RH.

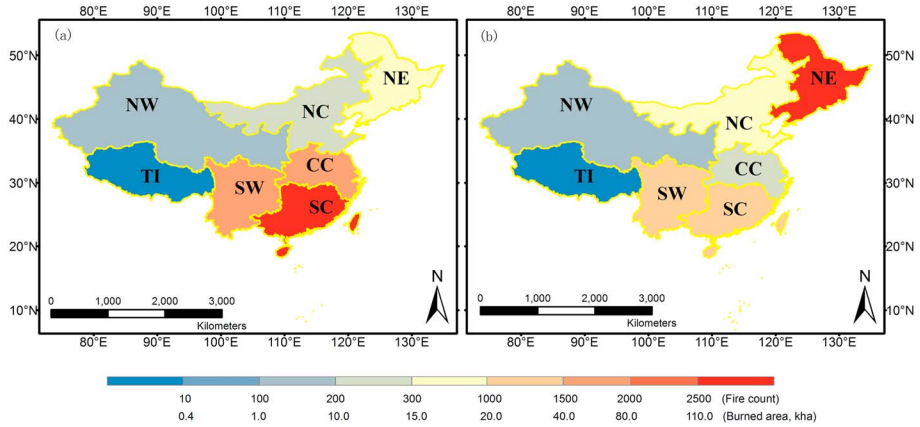

Figure 1. Regional distributions of annual forest fires in China. (a) Fire count and (b) burned area. The regions are northeast (NE), north (NC), central (cc), south (SC), and southwest (SW) China.

The circulation data used in this study were the global monthly gridded *Z*500 obtained from the National Centers for Environmental Prediction/Department of Energy Reanalysis-2 (https://rda.ucar.edu/datasets/ds091.1/) with a resolution of 2.5° (Kanamitsu et al., 2002). The major circulation systems are described in the supporting information (Figure S3). The impacts of El Niño–Southern Oscillation and Pacific Decadal Oscillation were not examined because they are low frequent fluctuations, while the data series used in this study was too short to conduct a statistical impact analysis.

2.3. Analysis Methods

The correlation coefficients between two time series A and B were calculated:

$$r_{j,m}(A,B) = \sum_{k=1}^{K} [A_m(k) \times B_m(k)] \tag{1}$$

where $A(k)$ and $B(k)$ were normalized over K (= 19) years for each month, m. $A = Z500$ at each grid point, and $B = F$ (= F_c, F_a), or *Met* (= T_{max}, RH) at an analyzed region, j. The $r_{j,m}$ (*Z*500, *F*) and $r_{j,m}$ (*Z*500, *Met*) were used to locate the geographical areas in Eurasia where the *Z*500 anomalies contributed to fires and weather, respectively, in a respective region of China. The two correlations were compared to understand the impacts of the identified circulation patterns on fire weather conditions.

Skinner et al. (2002) used a mean monthly zonal index, defined as the difference in *Z*500 between 45°N and 65°N, to characterize the type of circulation over a geographic region. This approach was adopted in this study to define two indices, ZI_{type} (*type* = *local*, *remote*) to explore the significance of the identified circulation patterns for fire predictions:

$$ZI_{local}(j,k) = Z500(j,k) - \overline{Z}500(j) \tag{2}$$

$$ZI_{remote}(j,k) = Z500(x_{max},k) - Z500(x_{min},k) \tag{3}$$

where x_{max} and x_{min} are the grid points with the maximum and minimum $r_{j,m}$ (*Z*500, *F*), respectively, near region j. $\overline{Z}$is averaged *Z*500 over years. The value of the indices for fire prediction was evaluated through two approaches: (1) comparing correlations with fires, $r_{j,m}$ (ZI_{type}, *F*), calculated by replacing *Z*500 with ZI_{type} in equation (1), with $r_{j,m}$ (*Met*, *F*); and (2) comparing fire predictions using univariable linear regression models with a circulation index and a local weather as predictor.

The univariable linear regression models for region j were formed as

$$y_j(t) = a_j + b_j\, x_j(t_{-1}) \tag{4}$$

where the dependent variable y_j is a fire property and the independent variable x_j is a circulation index or a meteorological element. t is a month during fire season and t_{-1} is a prior month. a_j is interception and b_j is

regression coefficient. Three models, Model0, Model1, and Model2, were developed using all 19 years (3 months in a year), the first 10 years and the last 9 years, respectively. The corresponding evaluation data were all years, the last 9 years and first 10 years. Each fire value in the evaluation series was classified into above normal if >avg + $c_1\sigma$, below if <avg − $c_2\sigma$, or normal otherwise, where avg and σ are average and standard deviation, respectively, $c_1 = 0.25$ and $c_2 = 0.5$ for F_c and $c_1 = 0.05$ and $c_2 = 0.25$ for F_a. The c_1 and c_2 values were selected so that the sample numbers in the three fire classes were as close as possible. The fitting rates for Model0 and prediction skills for Model1 and Model2 were measured by the number of the months in the evaluation data series when the observed and predicted fires fell into the same class of above normal.

3. Results and Discussion

3.1. Fire Features

F_c was much larger in southern China than in northern China, with the annual values averaged over the full period of 351 (NE), 230 (NC), 1,546 (CC), 2,935 (SC), and 1,854 ha (SW) (Figure 1). In contrast, F_a was generally larger in northern China than in southern China, with the annual values averaged over the full period of 118,693 (NE), 19,780 (NC), 10,257 (CC), 34,731 (SC), and 23,834 ha (SW). The wildfires in each region mainly occurred during the dry phase of a monsoon. The fire season (defined in this study as a 3-month period during a year with relatively large fire activities) was March–May in NE and NC and February–April in CC, SC, and SW. F_c and F_a during a fire season account for 64%–85% of the annual totals (Tables S1 and S2). The total annual F_c of all five regions was nearly 15,000 in 2004 and 2008 (Figure S2a), which was mainly attributed to the fires in SC during winter 2004 and spring 2008. The large total annual F_a was approximately 1,100 kha in 2003 and 600 kha in 2006 (Figure S2b), which was mainly attributed to the fires in NE during springs of the 2 years.

3.2. Circulation Patterns Associated With Wildfires

Three circulation patterns were identified according to the number and location of fire-$Z500$ correlation centers. The first pattern had a positive correlation center in NE (Figure 2), which was significant for March ($p < 0.001$) and April and May ($p < 0.01$). The second pattern had a mainly west-east oriented correlation dipole (i.e., a pair of positive and negative correlation centers) near NC, CC, or SC. The positive center on the western side was significant for February, March, and April in CC ($p < 0.05$) and February ($p < 0.1$) and March ($p < 0.05$) in SC. The negative center on the eastern side was significant for March ($p < 0.05$) and April ($p < 0.1$) in NC, February ($p < 0.01$), March ($p < 0.05$), and April ($p < 0.1$) in CC, and March ($p < 0.05$) in SC. The third pattern had a correlation dipole near SW. The negative center on the northwestern side was significant for February ($p < 0.05$) and April ($p < 0.001$). The positive center on the northeastern side was significant for March ($p < 0.1$) and April ($p < 0.001$).

The three patterns were closely linked to each other and corresponded to different status of the westerly systems. The monsoon regions of China are located between the westerly ridge in the west and the East Asian trough in the east (Figure S3). The first pattern suggests that wildfires in NE were more frequent when $Z500$ had positive anomalies in NE, which could happen when the ridge moved east. The positive and negative correlation centers with the second pattern approximately corresponded to the westerly ridge and trough areas, respectively. Both systems became stronger, meaning that the westerlies had a larger meridional component and that the stream became weaker when wildfires were more frequent in NC, CC, or SC. The negative and positive correlation centers with the third pattern approximately corresponded to the ridge and rough systems. Both became weaker, meaning that the westerly had a larger zonal component and that the stream became stronger when wildfires were more frequent in SW.

The circulation systems in the low latitudes, on the other hand, showed no close relationships with wildfires in most cases. The correlations had a large negative center in the northwestern Pacific Ocean subtropical high area only for the last month of fire season with the first and third circulation patterns. The negative sign indicated a weaker high-pressure system. Thus, the circulation patterns for wildfires were active mainly during the winter phase of the monsoon when the monsoon is driven mainly by the atmospheric circulation systems in the middle and high latitudes.

The links among the three circulation patterns were also seen from the relationships in large fires. The opposite changes in the westerly ridge and trough between the second and third patterns suggest potentially

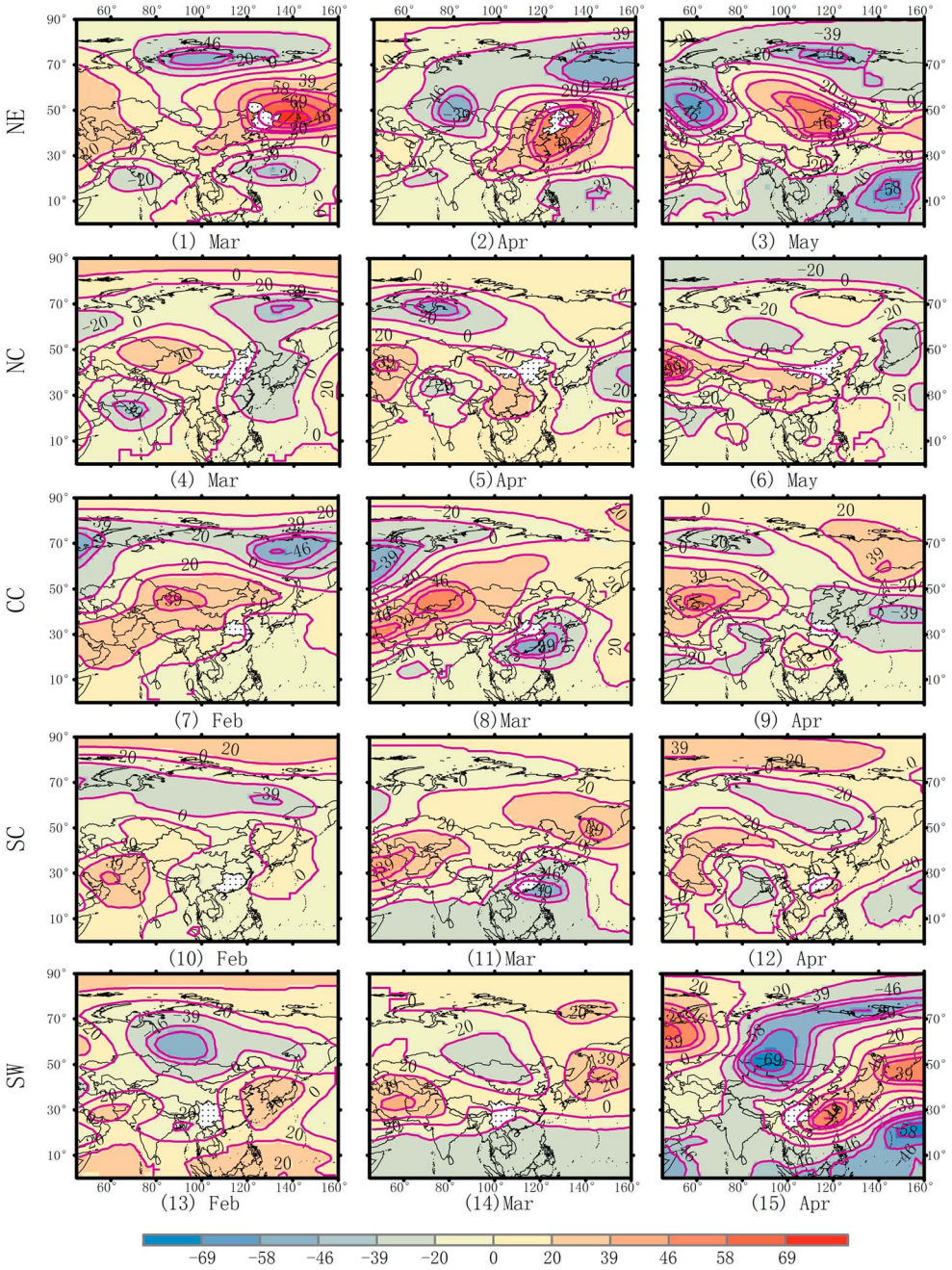

Figure 2. Correlation coefficients (%) between the 500-hPa geopotential height and the fire count of one of the NE (northeast), NC (north), CC (central), SC (south), and SW (southwest; white area with black dots) during 3 months of a fire season. The critical values (%) are 39 ($p < 0.1$), 46 ($p < 0.05$), 58 ($p < 0.01$), and 69 ($p < 0.001$).

opposite wildfire activities between SW and NC, CC, or SC, and the increasing $Z500$ in NE for the first pattern means a weaker westerly trough, suggesting similar fire activities between NE and SW and opposite ones between NE and NC, CC, or SC. These relationships were apparent in many years with large F_c (Figure S5), for example, February of 2010, March of 1999, and April of 2002 between CC and SW, and March of 2005, and April of 2003 between CC and NE.

The circulation patterns of $r_{j,m}$ ($Z500$, F_a; Figure S4) were similar to the corresponding patterns of $r_{j,m}$ ($Z500$, F_c). Th fire relationships among the three patterns were also found for F_a (Figure S5).

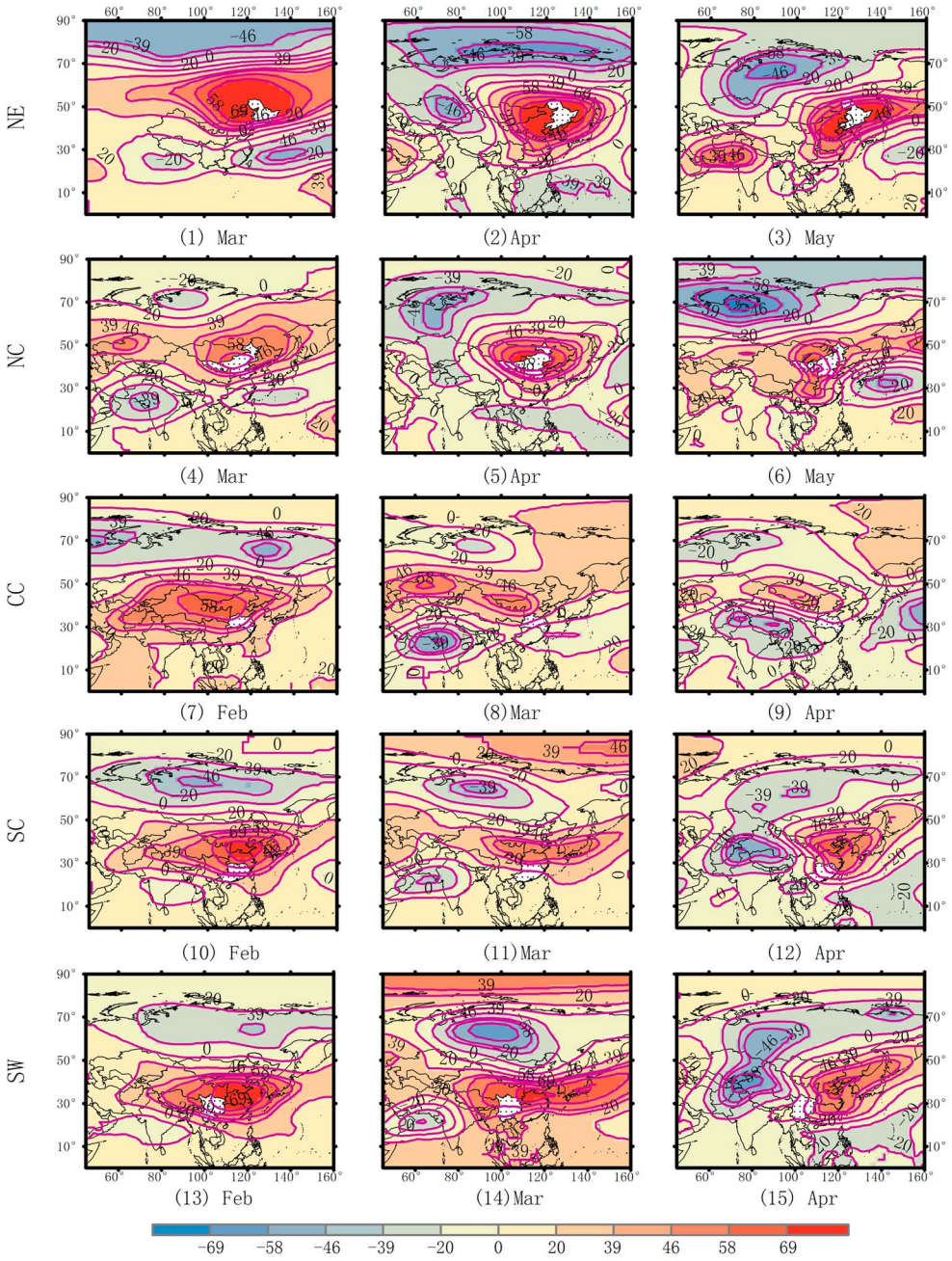

Figure 3. Same as Figure 2 except for correlation coefficients (%) between the temperature of a region (white area with black dots) and the 500-hPa geopotential height. NE = northeast; NC = north; CC = central; SC = south; SW = southwest.

We use "local" and "remote" to indicate a fire-*Z*500 correlation center that was and was not located within an analyzed wildfire region, respectively. Accordingly, the three patterns are then called as "local pattern," "remote meridional pattern," and "remote zonal pattern." The local pattern has been observed in, for example, Skinner et al. (1999). The remote meridional pattern is more or less similar to the first circulation empirical orthogonal function mode in the southcentral United States (Heilman, 1995). However, the center of the positive geopotential height anomalies with the mode is located in central California rather than in the westerly streams. The fire relationship of the meridional pattern is similar to a recent finding that maximum zonal North Pacific jet stream velocity is lower during presuppression high-fire extremes in California (Wahl et al., 2019). Trouet et al. (2018) found that the latitudinal position of the North Atlantic Jet can

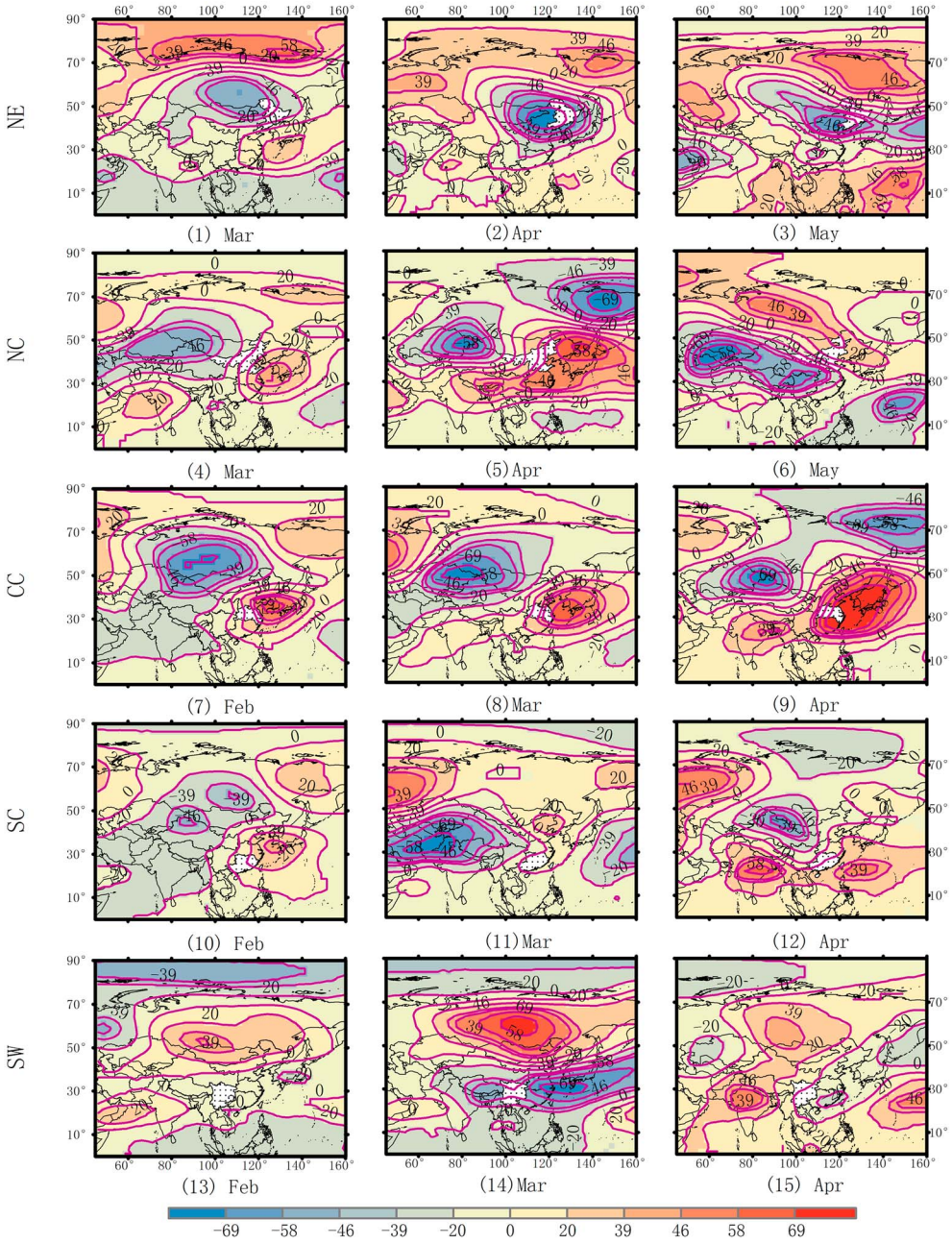

Figure 4. Same as Figure 2 except for correlation coefficients (%) between the relative humidity of a region (white area with black dots) and the 500-hPa geopotential height. NE = northeast; NC = north; CC = central; SC = south; SW = southwest.

affect wildfires in southeastern Europe. However, the impact of latitudinal position variability of the Euro-Asian westerly jet stream on wildfires in the monsoon regions of China was not examined in this study.

3.3. Impacts on Local Weather

The $r_{j,m}$ ($Z500$, T_{max}; Figure 3) had a region-independent pattern with a positive center in each region. In contrast, the $r_{j,m}$ ($Z500$, RH; Figure 4) had three patterns similar to those of $r_{j,m}$ ($Z500$, F_c) despite an opposite sign. This result, together with the result of the $r_{j,m}$ ($Z500$, F_c), indicates that when F_c was larger in NE, there were positive $Z500$ and T_{max} anomalies and negative RH anomalies in the region. A high-pressure system

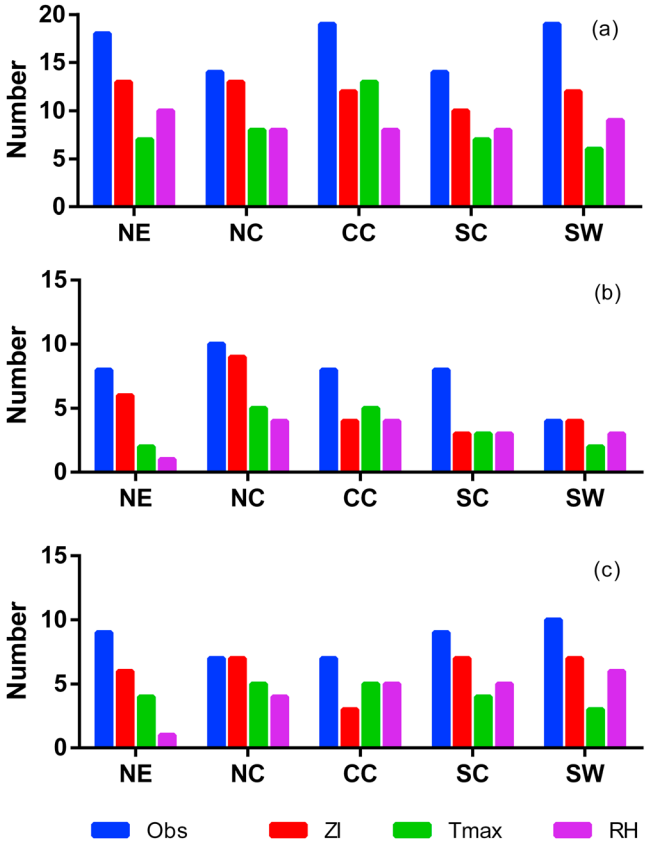

Figure 5. Prediction skills of monthly fire occurrence with Model0 (a), Model1 (b), and Model3 (c). The fire regions are NE (northeast), NC (north), CC (central), SC (south), and SW (southwest) China. Blue is the observed number of fires in the above normal class. Red, green, and purple are the numbers of predicted fires that are also in the above normal class using the remote circulation index, maximum temperature, and relative humidity as a predictor, respectively.

produces air subsidence, which warms air adiabatically and decreases the relative humidity (https://www.sciencedirect.com/topics/earth-and-planetary-sciences/high-pressure-system). Thus, the first circulation pattern contributed to wildfires in NE by producing warmer and drier local weather.

When F_c was larger in NC, CC, or SC, $Z500$ anomalies were positive (negative) in the west and negative in the east of each region, while RH anomalies were negative in the west and positive in the east. In the west, the stronger ridge led to stronger inner-continental dry airflows; in the east, the stronger trough led to more dry airflows from the high latitudes and less moist airflows from the low latitudes. These changes in the west increased transport of drier air to the fire region.

When F_c was larger in SW, $Z500$ anomalies were negative in the northern or northwestern parts of the region, while RH anomalies were positive in the northern or northwestern parts, which contributed to wildfires in SW by blocking the transport of dry air from the north. This scenario may imply more warm and moist air transport from the low latitudes, which contributes to increasing lightning fire activity (García-Ortega et al., 2011; Peterson et al., 2010; Xia et al., 2018).

3.4. Circulation Indices

The $r_{j,m}$ (ZI_{remote}, F_c) was significant ($p < 0.1$ or higher) in all regions except for February in SC (Figure S6). In all 15 cases (five regions × 3 months), the $r_{j,m}$ (ZI_{remote}, F_c) was larger than or comparable to $r_{j,m}$ ($T_{\max}$, F_c) and $r_{j,m}$ (RH, F_c) in 14 cases. The $r_{j,m}$ (ZI_{local}, F_c), on the other hand, was significant ($p < 0.1$) only in NE, in agreement with $r_{j,m}$ ($Z500$, F_c). The $r_{NE,m}$ (ZI_{local}, F_c) and $r_{NE,m}$ (ZI_{remote}, F_c) were close in magnitude. The $r_{NE,m}$ (ZI_{local}, F_c) was larger than or comparable to $r_{NE,m}$ ($T_{\max}$, F_c) and $r_{NE,m}$ (RH, F_c), except for RH in May. Similar results are seen for F_a. Table S3 lists the months with significant correlations to help fire managers select fire predictors.

The three regression models showed overwhelmingly higher prediction skills for above normal F_c using ZI_{remote} than $T_{\max}$ or RH (Figure 5). For Model0, the observed total F_c of the five regions was 84; the model F_c was 60, 41, and 43 using ZI_{remote}, $T_{\max}$, and RH as a predictor, respectively. Thus, the fitting rates were 71%, 49%, and 51%. The corresponding F_c was 38, 26, 17, and 15 (the correction rates of 68%, 45%, and 39%) for Model1 and 42, 30, 21, and 21 (the correction rates of 71%, 50%, and 50%) for Model2.

However, the regression models showed no strong differences in skills for the class of above normal F_a between ZI_{remote} and $T_{\max}$ or RH. China has implemented a strict forest fire suppression policy (Zhao et al., 2009) since the catastrophic Black Dragon Fire in the Daxing'an Mountains in May 1987 (Cahoon et al., 1994). The impacts of this human factor may have made F_c less related to natural processes.

4. Conclusions

Three atmospheric circulation patterns were identified for wildfires in the monsoon regions of China. A local circulation pattern of positive geopotential height anomalies contributed to wildfires in northeast China by generating warmer and drier local conditions. A remote meridional pattern of stronger westerly ridge and trough contributed to wildfires in north, central, and south China by increasing transport of dry air. A remote zonal pattern of weaker westerly ridge and trough contributed to wildfires in southwest China by blocking the transport of dry air.

These circulation patterns have important implications for fire predictions. Monthly occurrence of large fires were better predicted using the remote circulation index based on the circulation patterns than local weather

in most monsoon regions of China. Furthermore, large regional fire activities under the control of different circulation patterns are often interrelated.

Acknowledgments
We thank Shela Mou for English edits. Fire statistics are provided in the supporting information. The original fire and weather data can be accessed at the websites provided in this paper (the fire website requires registration). This study was supported by China National Key Research and Development Plan (2017YFD0600106), China Natural Science Foundation (project 31670661), and USDA Forest Service. The authors do not have a conflict of interest.

References

Abatzoglou, J. T., & Williams, A. P. (2016). Impact of anthropogenic climate change on wildfire across western US forests. *Proceedings of the National Academy of Sciences*, *113*(42), 11,770–11,775. https://doi.org/10.1073/pnas.1607171113

Amraoui, M., Liberato, M. L. R., Calado, T. J., DaCamara, C. C., Coelho, L. P., Trigo, R. M., & Gouveia, C. M. (2013). Fire activity over Mediterranean Europe based on information from Meteosat-8. *Forest Ecology and Management*, *294*, 62–75. https://doi.org/10.1016/j.foreco.2012.08.032

Amraoui, M., Pereira, M. G., DaCamara, C. C., & Calado, T. J. (2015). Atmospheric conditions associated with extreme fire activity in the Western Mediterranean region. *Science of the Total Environment*, *524-525*, 32–39. https://doi.org/10.1016/j.scitotenv.2015.04.032

Cahoon, D. R., Stocks, B. J., Levine, J. S., Cofer, W. R. III, & Pierson, J. M. (1994). Satellite analysis of the severe 1987 forest fires in northern China and southeastern Siberia. *Journal of Geophysical Research*, *99*(D9), 18,627–18,638. https://doi.org/10.1029/94JD01024

Chang, Y., Zhu, Z. L., Bu, R., Li, Y. H., & Hua, Y. M. (2015). Environmental controls on the characteristics of mean number of forest fires and mean forest area burned (1987–2007) in China. *Forest Ecology and Management*, *356*, 13–21. https://doi.org/10.1016/j.foreco.2015.07.012

Chang, Y., Zhu, Z. L., Bu, R. C., Chen, H. W., Feng, Y. T., Li, Y. H., et al. (2013). Predicting fire occurrence patterns with logistic regression in Heilongjiang Province, China. *Landscape Ecology*, *28*(10), 1989–2004. https://doi.org/10.1007/s10980-013-9935-4

Chen, D. M., Pereira, J. M. C., Masiero, A., & Pirotti, F. (2017). Mapping fire regimes in China using MODIS active fire and burned area data. *Applied Geography*, *85*, 14–26. https://doi.org/10.1016/j.apgeog.2017.05.013

Ding, Y. H., & Chan, J. C. L. (2005). The East Asian summer monsoon: An overview. *Meteorology and Atmospheric Physics*, *89*(1-4), 117–142. https://doi.org/10.1007/s00703-005-0125-z

Doerr, S., & Santín, C. (2016). Global trends in wildfire and its impacts: Perception versus realities in a changing world. *Philosophical Transactions of the Royal Society B*, *371*(1696), 20150345. https://doi.org/10.1098/rstb.2015.0345

Fauria, M. M., & Johnson, E. A. (2006). Large-scale climatic patterns control large lightning fire occurrence in Canada and Alaska forest regions. *Journal of Geophysical Research*, *111*, G04008. https://doi.org/10.1029/2006JG000181

Flannigan, M. D., Krawchuk, M. A., de Groot, W. J., Wotton, M., & Gowman, L. M. (2009). Implications of changing climate for global wildland fire. *International Journal of Wildland Fire*, *9*(18), 483–507. https://doi.org/10.1071/WF08187

Founda, D., & Giannakopoulos, C. (2009). The exceptionally hot summer of 2007 in Athens, Greece—A typical summer in the future climate? *Global and Planetary Change*, *67*(3-4), 227–236. https://doi.org/10.1016/j.gloplacha.2009.03.013

García-Ortega, E., Trobajo, M. T., Lopez, L., & Sanchez, J. L. (2011). Synoptic patterns associated with wildfires caused by lightning in Castile and Leon, Spain. *Natural Hazards and Earth System Sciences*, *11*(3), 851–863. https://doi.org/10.5194/nhess-11-851-2011

Gill, A. M., & Stephens, S. L. (2009). Scientific and social challenges for the management of fire-prone wildland–urban interfaces. *Environmental Research Letters*, *4*(3), 034014. https://doi.org/10.1088/1748-9326/4/3/034014

Ha, K. J., Heo, K. Y., Lee, S. S., Yun, K. S., & Jhun, J. G. (2012). Variability in the East Asian Monsoon: A review. *Meteorological Applications*, *19*(2), 200–215. https://doi.org/10.1002/met.1320

Hayasaka, H., Tanaka, H. L., & Bieniek, P. A. (2016). Synoptic-scale fire weather conditions in Alaska. *Polar Science*, *10*(3), 217–226. https://doi.org/10.1016/j.polar.2016.05.001

Heilman, W. E. (1995). Synoptic circulation and temperature patterns during severe wildland fires. In *"Proceedings of the Ninth Conference on Applied Climatology", 15–20 January 1995, Dallas, TX* (pp. 346–351). Boston, MA: American Meteorological Society.

Hostetler, S. W., Bartlein, P. J., & Alder, J. R. (2018). Atmospheric and surface climate associated with 1986–2013 wildfires in North America. *Journal of Geophysical Research: Biogeosciences*, *123*, 1588–1609. https://doi.org/10.1029/2017JG004195

Huang, R. H., Liu, Y., Du, Z. C., Chen, J. L., & Huangfu, J. L. (2017). Differences and links between the East Asian and South Asian summer monsoon systems: Characteristics and variability. *Advances in Atmospheric Sciences*, *34*(10), 1204–1218. https://doi.org/10.1007/s00376-017-7008-3

Kanamitsu, M., Ebisuzaki, W., Woollen, J., Yang, S. K., Hnilo, J. J., Fiorino, M., & Potter, G. L. (2002). NCEP-DOE AMIP-II reanalysis (R-2). *Bulletin of the American Meteorological Society (BAMS)*, *83*(11), 1631–1644. https://doi.org/10.1175/BAMS-83-11-1631

Lagerquist, R., Flannigan, M. D., Wang, X. L., & Marshall, G. A. (2017). Automated prediction of extreme fire weather from synoptic patterns in northern Alberta, Canada. *Canadian Journal of Forest Research*, *47*(9), 1175–1183. https://doi.org/10.1139/cjfr-2017-0063

Li, J. F., Song, Y., Huang, X., & Li, M. M. (2015). Comparison of forest burned areas in mainland China derived from MCD45A1 and data recorded in yearbooks from 2001 to 2011. *International Journal of Wildland Fire*, *24*(1), 103–113. https://doi.org/10.1071/WF14031

Li, X. W., Zhao, G., Yu, X. B., & Yu, Q. (2014). A comparison of forest fire indices for predicting fire risk in contrasting climates in China. *Natural Hazards*, *70*(2), 1339–1356. https://doi.org/10.1007/s11069-013-0877-6

Liu, Y. Q., Goodrick, S. L., & Heilman, W. (2014). Wildland fire emissions, carbon, and climate: Wildfire-climate interactions. *Forest Ecology and Management*, *317*, 80–96. https://doi.org/10.1016/j.foreco.2013.02.020

Lv, A. F., Tian, H. Q., Liu, M. L., Liu, J. Y., & Melillo, J. M. (2006). Spatial and temporal patterns of carbon emissions from forest fires in China from 1950 to 2000. *Journal of Geophysical Research*, *111*, D05313. https://doi.org/10.1029/2005JD006198

Moritz, M. A., Batllori, E., Bradstock, R. A., Malcolm, G. A., Handmer, J., Hessburg, P. F., et al. (2014). Learning to coexist with wildfire. *Nature*, *515*(7525), 58–66. https://doi.org/10.1038/nature13946

Nagy, R. C., Fusco, E., Bradley, B., Abatzoglou, J. T., & Balch, J. (2018). Human-related ignitions increase the number of large wildfires across U.S. ecoregions. *Fire*, *1*(1), 4. https://doi.org/10.3390/fire1010004

Nauslar, N. J., Abatzoglou, J. T., & Marsh, P. T. (2018). The 2017 North Bay and Southern California fires: A case study. *Fire*, *1*(1), 18. https://doi.org/10.3390/fire1010018

Niu, R. Y., & Zhai, P. (2012). Study on forest fire danger over northern China during the recent 50 years. *Climatic Change*, *111*(3-4), 723–736. https://doi.org/10.1007/s10584-011-0198-2

O'Donnell, A. J., Boer, M. M., Mccaw, W. L., & Grierson, P. F. (2011). Climatic anomalies drive wildfire occurrence and extent in semi-arid shrublands and woodlands of southwest Australia. *Ecosphere*, *2*(11), 1–15. https://doi.org/10.1890/ES11-00189.1

Papadopoulos, A., Paschalidou, A. K., Kassomenos, P. A., & McGregor, G. (2014). On the association between synoptic circulation and wildfires in the Eastern Mediterranean. *Theoretical and Applied Climatology*, *115*(3-4), 483–501. https://doi.org/10.1007/s00704-013-0885-1

Paschalidou, A. K., & Kassomenos, P. A. (2016). What are the most fire-dangerous atmospheric circulations in the Eastern-Mediterranean? Analysis of the synoptic wildfire climatology. *Science of the Total Environment*, *539*, 536–545. https://doi.org/10.1016/j.scitotenv.2015.09.039

Pereira, M. G., Trigo, R. M., da Camara, C. C., Pereira, J. M. C., & Leite, S. M. (2005). Synoptic patterns associated with large summer forest fires in Portugal. *Agricultural and Forest Meteorology*, *129*(1-2), 11–25. https://doi.org/10.1016/j.agrformet.2004.12.007

Peterson, D., Wang, J., Ichoku, C., & Remer, L. A. (2010). Effects of lightning and other meteorological factors on fire activity in the North American boreal forest: Implications for fire weather forecasting. *Atmospheric Chemistry and Physics*, *10*(14), 6873–6888. https://doi.org/10.5194/acp-10-6873-2010

Ruffault, J., Moron, V., Trigo, R. M., & Curt, T. (2017). Daily synoptic conditions associated with large fire occurrence in Mediterranean France: Evidence for a wind-driven fire regime. *International Journal of Climatology*, *37*(1), 524–533. https://doi.org/10.1002/joc.4680

Schoennagel, T., Balch, J. K., Brenkert-Smith, H., Dennison, P. E., Harvey, B. J., Krawchuk, M. A., et al. (2017). Adapt to more wildfire in western North American forests as climate changes. *Proceedings of the National Academy of Sciences*, *114*, 4582–4590. https://doi.org/10.1073/pnas.1617464114

Skinner, W. R., Flannigan, M. D., Stocks, B. J., Martell, D. L., Wotton, B. M., Todd, J. B., et al. (2002). A 500 hPa synoptic wildland fire climatology for large Canadian forest fires, 1959–1996. *Theoretical and Applied Climatology*, *71*(3-4), 157–169. https://doi.org/10.1007/s007040200002

Skinner, W. R., Stocks, B. J., Martell, D. L., Bonsal, B., & Shabbar, A. (1999). The association between circulation anomalies in the mid-troposphere and area burned by wildland fire in Canada. *Theoretical and Applied Climatology*, *63*(1-2), 89–105. https://doi.org/10.1007/s007040050095

Steelman, T. (2016). U. S. wildfire governance as social-ecological problem. *Ecology and Society*, *21*(4), 3. https://doi.org/10.5751/ES-08681-210403

Sun, P., & Zhang, Y. L. (2018). A probabilistic method predicting forest fire occurrence combining firebrands and the weather-fuel complex in the northern part of the Daxinganling region, China. *Forests*, *9*(7), 428. https://doi.org/10.3390/f9070428

Tian, X. R., Zhao, F. J., Shu, L. F., & Wang, M. Y. (2013). Distribution characteristics and the influence factors of forest fires in China. *Forest Ecology and Management*, *310*, 460–467. https://doi.org/10.1016/j.foreco.2013.08.025

Trouet, V., Babst, F., & Meko, M. (2018). Recent enhanced high-summer North Atlantic Jet variability emerges from three-century context. *Nature Communications*, *9*(1), 180. https://doi.org/10.1038/s41467-017-02699-3

Trouet, V., Taylor, A. H., Carleton, A. M., & Skinner, C. N. (2009). Interannual variations in fire weather, fire extent, and synoptic-scale circulation patterns in northern California and Oregon. *Theoretical and Applied Climatology*, *95*(3-4), 349–360. https://doi.org/10.1007/s00704-008-0012-x

Turco, M., Jerez, S., Doblas-Reyes, F. J., Kouchak, A. A., Llasat, M. C., & Provenzale, A. (2018). Skillful forecasting of global fire activity using seasonal climate predictions. *Nature Communications*, *9*(1), 2718. https://doi.org/10.1038/s41467-018-05250-0

Wahl, E. R., Zorita, E., Trouet, V., & Taylor, A. H. (2019). Jet stream dynamics, hydroclimate, and fire in California from 1600 CE to present. *PNAS*, *116*(12), 5393–5398. https://doi.org/10.1073/pnas.1815292116

Westerling, A. L., Hidalgo, H. G., Cayan, R., & Swetnam, T. W. (2006). Warming and earlier spring increase western U.S. forest wildfire activity. *Science*, *313*(5789), 940–943. https://doi.org/10.1126/science.1128834

Wise, E. K. (2016). Five centuries of U.S. west coast drought: Occurrence, spatial distribution, and associated atmospheric circulation patterns. *Geophysical Research Letters*, *43*, 4539–4546. https://doi.org/10.1002/2016GL068487

Xia, R. D., Zhang, D. L., Zhang, C. H., & Wang, Y. Q. (2018). Synoptic control of convective rainfall rates and cloud to ground lightning frequencies in warm-season mesoscale convective systems over North China. *Monthly Weather Review*, *146*(3), 813–831. https://doi.org/10.1175/MWR-D-17-0172.1

Yao, Q. C., Brown, P. M., Liu, S., Rocca, M. E., Trouet, V., Zheng, B., et al. (2017). Pacific-Atlantic Ocean influence on wildfires in northeast China (1774 to 2010). *Geophysical Research Letters*, *44*, 1025–1033. https://doi.org/10.1002/2016GL071821

Yi, K. P., Bao, Y. L., & Zhang, J. Q. (2017). Spatial distribution and temporal variability of open fire in China. *International Journal of Wildland Fire*, *26*(2), 122–135. https://doi.org/10.1071/WF15213

Zhang, Y. J., Qin, D. H., Yuan, W. P., & Jia, B. R. (2016). Historical trends of forest fires and carbon emissions in China from 1988 to 2012. *Journal of Geophysical Research: Biogeosciences*, *121*, 2506–2517. https://doi.org/10.1002/2016JG003570

Zhao, F. J., Shu, L. F., Di, X. Y., Tian, X. R., & Wang, M. Y. (2009). Changes in the occurring date of forest fires in the Inner Mongolia Daxing'anling forest region under global warming (in Chinese). *Scientia Silvae Sinica*, *45*(6), 166–172. https://doi.org/10.11707/j.1001-7488.20090630